

Excitation function for $^{nat}\text{Mo}(p,x)$ reactions with covariance analysis

Sumit Bamal¹, S. Lawitlang², B. Lalremruata², A. Mazumdar³, S. Pal⁴, M. S. Pose⁵, V. Nanal⁵ ^a, and Rebecca Pachuau¹ ^b

¹ Department of Physics, Banaras Hindu University, Varanasi-221005, INDIA

² Department of Physics, Mizoram University, Aizawl - 796004, INDIA

³ INO, Tata Institute of Fundamental Research, Mumbai - 400005, INDIA ^c

⁴ PLF, Tata Institute of Fundamental Research, Mumbai - 400005, INDIA

⁵ DNAP, Tata Institute of Fundamental Research, Mumbai - 400005, INDIA

Received: date / Revised version: date

Abstract. The excitation functions of proton induced reactions on ^{nat}Mo targets are measured using the activation technique followed by off-line γ -ray spectroscopy with improved precision. The experiment was performed at the BARC-TIFR Pelletron Linac Facility, Mumbai. Thin samples of ^{nat}Mo were irradiated with a proton beam of energies ranging from 13 to 22 MeV for measurements of various (p,x) cross sections, with an emphasis on the production of medical isotopes. The present data for ^{93m}Tc and ^{94g}Tc address and resolve the discrepancies in the existing data. The ^{93g}Tc radioisotope production is extracted with appropriate corrections for ^{93m}Tc contribution. While the measured cross sections for the production of ^{95g}Tc , $^{96g+m}\text{Tc}$, ^{99m}Tc and ^{99}Mo are consistent with the reported data, significant differences are observed for $^{89g+m}\text{Zr}$. A comprehensive uncertainty analysis, including the correlation coefficients of the measured reaction cross sections is also presented.

PACS. 2 5.40.Lw, 25.40.-h, 24.50.+g

1 Introduction

Proton induced reactions are of great importance in various fields including nuclear medicine [1], theranostics applications [2], astrophysical p-processes [3] and as variable energy neutron sources for research purposes. The importance of radioisotopes for theranostics in modern healthcare cannot be overemphasized. Presently, there are around 200 artificially produced medical isotopes, which are used in various medical procedures [2]. Innovative ways for medical isotope manufacturing are also being studied, including laser isotope separation and photo plasma creation [4]. Proton induced reactions on Molybdenum are of interest for the production of radioisotopes for a wide variety of medical applications such as detection of cancer, heart disease, kidney disease, bone disorders, salivary gland disorders, thyroid disorders, PET (Positron Emission Tomography) scans and SPECT (Single Photon Emission Computed Tomography) scans.

A range of radioisotopes ^{99m}Tc , ^{99}Mo , ^{96g}Tc , ^{95g}Tc , ^{94g}Tc , and ^{89g}Zr can be produced in $^{nat}\text{Mo}(p,x)$ reactions. Among these, the ^{99m}Tc holds significant importance as it alone accounts for approximately 80% of all nuclear medicinal procedures. The ^{99m}Tc finds extensive application in SPECT imaging, particularly in diagnosing strokes. The ideal properties of ^{99m}Tc include its appropriate half-life, penetrating strength, and minimal biological damage from administered doses, making it a valuable radiopharmaceutical for various diagnostic purposes. Further, its nuclear properties also make it ideal for medical imaging due to its relatively high photon energy (≈ 140 keV), which allows a precise determination of molecular structure using scintillation devices like gamma cameras [5].

Given the critical role of medical radioisotope ^{99m}Tc , there is a wide interest for potential alternatives. In this context, Takehito Hayakawa et al. [6] have proposed that the radioisotopes ^{96g}Tc and ^{95g}Tc could serve as viable substitutes for ^{99m}Tc as γ -ray emitters. The long-lived positron emitter ^{89g}Zr ($T_{1/2} = 78.41$ hrs) is significant in immuno-PET scans due to its favorable physical characteristics [2]. The ^{94g}Tc can be used in PET imaging technique as a carrier-free radionuclide. Accurate cross section data are essential for these radioisotopes for pro-

^a e-mail: nanal@tifr.res.in

^b e-mail: pcr1.bec@gmail.com

^c Presently at Department of Physics and Astronomy, University of North Carolina, Chapel Hill, NC 27599, USA

posed applications in medical diagnostics. [7]. Production of ^{99}Mo has traditionally relied on reactor-based routes, either via neutron capture on ^{98}Mo ($^{98}\text{Mo}(\text{n},\gamma)^{99}\text{Mo}$) or as a fission product in highly enriched uranium (HEU) targets. However, increasing restrictions on the use of HEU and the growing global demand for $^{99\text{m}}\text{Tc}$ have motivated the development of accelerator based production strategies [8], employing protons, deuterons, or electron beams on molybdenum targets. Hence, accelerator based production of ^{99}Mo offers a sustainable and reactor independent alternative that is directly relevant to nuclear medicine supply security. The radionuclide ^{99}Mo decays via β^- emission to produce the clinically important $^{99\text{m}}\text{Tc}$, making it a convenient parent for the on-demand $^{99\text{m}}\text{Tc}$ generators. It should be noted that cross-disciplinary research not only advances medical science, but also yields important inputs for nuclear reaction mechanism.

Further, $\text{Mo}(\text{p},\text{x})$ data may be important for nuclear technology applications. With a melting point of 2623 °C and thermal conductivity of 112 W/m·K at 1000 K, molybdenum is compatible with both water and liquid-metal coolants. As a result, it is suitable for advanced fuel element structures. Relative to zirconium, it reduces the thermal time constant of fuel rods by nearly a factor of two, which improves reactivity feedback and safety margins [9,10]. In dispersion fuels, U–Mo alloy granules in a molybdenum matrix provide high fissile density and efficient heat transfer, maintaining stability at high burn-up [10].

Precise determination of nuclear reaction cross sections and incident proton energies is essential for improving the reliability of experimental results and for benchmarking theoretical models. Low uncertainty in these quantities enables accurate comparison between experimental data and model calculations, which is particularly important for applications such as medical isotope production and nuclear data evaluations. In addition to minimizing statistical and systematic uncertainties, it is important to include covariance and correlation information when reporting cross section data. This becomes especially relevant when the data are used for interpolation or extrapolation across energy ranges where measurements are not directly available. Covariance matrices provide a quantitative representation of how uncertainties at different energy points are related. Ignoring these correlations can lead to incorrect uncertainty propagation and potentially misleading results, especially when integrated cross sections or model fits are involved. Therefore, including detailed uncertainty analysis along with covariance and correlation data significantly enhances the utility and reliability of nuclear reaction data for both experimental and theoretical purposes. However, the existing datasets in the EXFOR database are limited and show some discrepancies. Moreover, most of the data is from thick target irradiation and consequently have a large spread in incident beam energy. Hence, there is a need for additional measurements with high precision, which can be achieved with thin targets. With this motivation, in the present work, the excitation functions for various radioisotopes produced in

$^{nat}\text{Mo}(\text{p},\text{x})$ reactions are measured over an incident beam energy range of 12 to 22 MeV with improved precision. In addition, a detailed uncertainty propagation and covariance analysis is also carried out. The correlation coefficients between incident proton energy and cross section of nuclear reactions are not only useful for optimization of production of isotope of interest, but can also provide insights into reaction mechanisms.

This paper is organised as follows. The experimental details are described in section 2, analysis procedure is given in section 3, the results on production of various isotopes are given in section 4 and the conclusions are given in the last section.

2 Experimental details

The experiment was performed at 14UD BARC-TIFR Pelletron Linac Facility in Mumbai, where high purity ($\approx 99.9\%$) natural molybdenum foils were irradiated with the proton beams of energy ~ 12 to 22 MeV. The thickness of Mo targets was in the range 7.79 - 10.34 mg/cm². For efficient use of beam time, the irradiation was combined with another experiment and a stack of Zr-Cu-Mo foils was used in each run. Average thickness of the individual target foils was determined by measuring its mass and area, assuming uniformity. The average beam energy in the lab frame, at the center of each Mo target foil, and the spread in the energy due to target thickness were calculated using the SRIM code [11]. The uncertainty in the incident beam energy, including effects of cascaded targets, is $\sim 0.060 - 0.085$ MeV. Details of irradiation are given in Table 1.

Table 1: Details of irradiation : Proton energy (E_p) in center of mass frame at the center of the Mo target, target thickness, irradiation time (T_{irr}) and average beam current (I).

E_p (MeV)	Mo Thickness (mg/cm ²)	T_{irr} (hrs)	I (nA)
21.54±0.06	8.30±0.04	1.25	100
19.63±0.08	9.81±0.04	1.01	92
18.54±0.06	7.79±0.05	1.05	99
17.73±0.08	9.95±0.04	1.02	62
16.54±0.07	8.12±0.05	0.82	111
15.71±0.09	10.23±0.05	1.53	58
13.53±0.08	8.28±0.04	1.93	62
12.57±0.08	7.83±0.04	1.70	97

The incident proton flux was calculated from the charge (Q) collected on the Faraday cup situated downstream of the target. To correct for beam fluctuations during the irradiation ($\sim 28\%$), incident charge (beam current) was recorded at regular intervals of 10 to 60 seconds. A suitable cool-down time was allowed to ensure the permissible radioactive dose levels for handling the irradiated targets

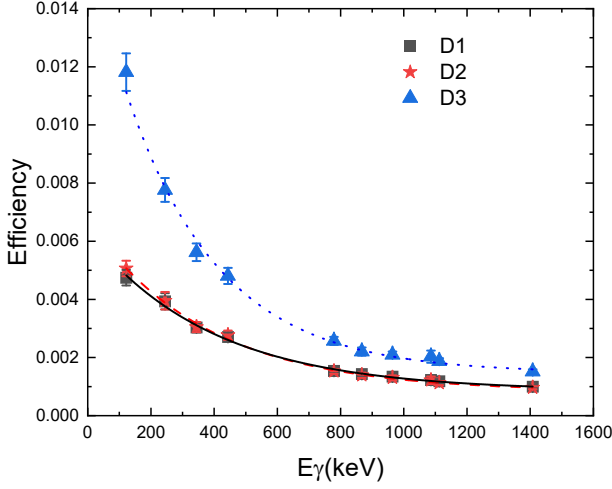


Fig. 1: Absolute detector efficiency of HPGe detectors as a function of energy along with the fitted curves.

during counting.

Three HPGe detectors were used for offline measurements of γ -ray spectra of the various irradiated samples- Detectors D1 and D2 with relative efficiency of 38% (Bruker Baltic make), and detector D3 with relative efficiency of 30% (ORTEC make) These detectors were calibrated using a standard ^{152}Eu source (20105 ± 1005 Bq). Irradiated targets were mounted at a distance of ~ 10 cm from the face of the HPGe detector and efficiency was measured in identical geometry for all three detectors. The spectra were recorded using a CAEN N6724 digitizer and analyzed offline using the Linux Advanced MultiParameter System (LAMPS) software [12].

The absolute detector efficiency of $\epsilon(E_\gamma)$ corresponding to various gamma rays observed from the ^{152}Eu source was calculated using the equation:

$$\epsilon(E_\gamma) = \frac{N_\gamma}{N_0 I_\gamma t_m}, \quad (1)$$

where N_0 is the source activity, N_γ and I_γ are the photopeak counts and branching ratio of γ ray of interest, and t_m is the counting time. The efficiency data was fitted to an exponential function:

$$\epsilon(E_\gamma(i)) = \epsilon_0 \exp(-E_\gamma(i)/E_0) + \epsilon_c, \quad (2)$$

where ϵ_0 , E_0 (keV) and ϵ_c are the fitting parameters of the equation. together with fitted functions are shown in Figure 1 for all the three detectors (D1, D2 and D3). The fitting parameters together with the covariance matrix are listed in Table 2.

3 Data Analysis

The reactions products were identified by the dominant characteristic gamma rays. Table 3 gives a summary of the observed reaction channels and corresponding dominant gamma rays used for the cross section calculation. To ensure unique identification of reaction products, half-life was tracked by recording data at suitable time intervals. As a typical example, the measured half-life data for ^{95g}Tc and ^{96g}Tc is shown in Figure 2. The measured half-life values ($T_{1/2}^{expt}$) for all observed channels are found to be consistent with literature values (within measurement errors) and are also listed in Table 3.

3.1 cross section measurement

The production cross section of a given nuclide is calculated using the equation:

$$\sigma = \frac{N_\gamma \lambda}{N_t a \epsilon N_p I_\gamma T_f}, \quad (3)$$

where N_γ , I_γ , ϵ are the photopeak intensity, branching ratio and photopeak efficiency of the characteristic γ -ray, respectively, λ is the decay constant, N_t is the number of target atoms per unit area, a is natural isotopic abundance of the parent isotope, N_p is the number of protons incident per second on the target. The timing factor T_f , which is a correction for the decay during the irradiation and cooldown time, is given by eqn.(4):

$$T_f = (1 - e^{-\lambda t_{irr}}) e^{-\lambda t_{cool}} (1 - e^{-\lambda t_{count}}), \quad (4)$$

where t_{irr} is irradiation time, t_{cool} is the cooling time and t_{count} is the counting time.

The irradiation time is considered as $t_{irr} = \sum_1^n dt(i)$ such that $dt(i) \sim 10-60\text{sec} \ll T_{1/2}$. As mentioned earlier the charge incident on the target $dq(i)$ was recorded for each interval. To take care of the effects of beam current fluctuations, the cross section was obtained by computing the production of the radionuclide in each interval for incident charge $dq(i)$ and correcting for the decay of the radionuclide during the time interval $dt(i)$.

Let $K = a N_t \sigma / e$ be the number of nuclei produced per unit charge, where e is the electronic charge. $P(i)$, which is the number of nuclei produced in the i^{th} interval, can then be written as

$$P(i) = K dq(i) = \frac{a N_t \sigma}{e} dq(i) \quad (5)$$

Considering the decay of radionuclide during the same interval, the net yield $Y(i)$ can be expressed as

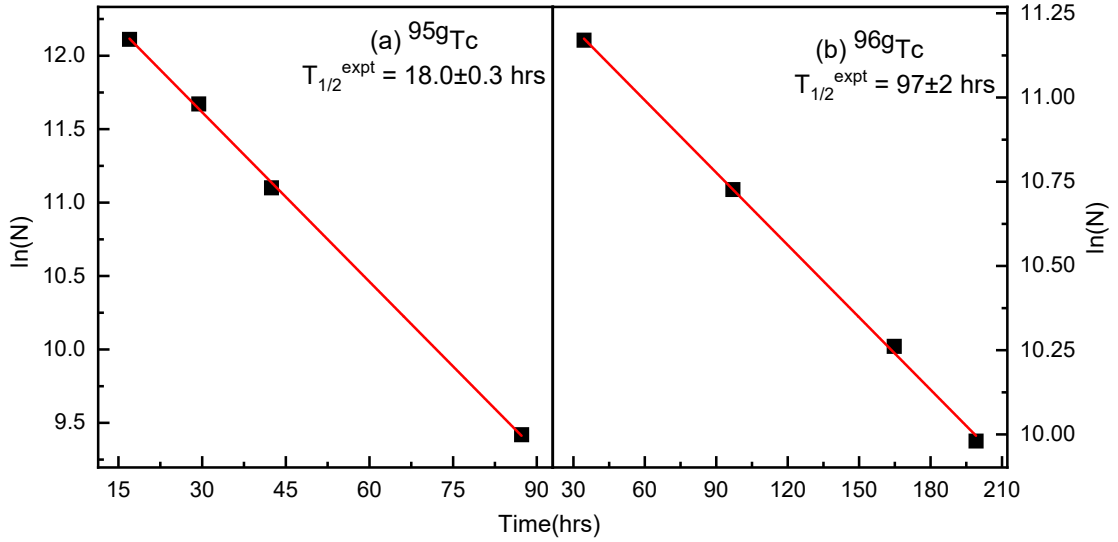
$$Y(i) = Y(i-1) + P(i) - \lambda_m Y(i-1) = K \cdot X(i)$$

The quantity $X(i)$ is computed for each interval and the yield at the end of irradiation is obtained

$$Y(n) = K \cdot X(n)$$

Table 2: Fitting parameters of efficiency curves and covariance matrix for the detectors.

Detector	Parameters	Value	Covariance Matrix			
D1	ϵ_c	$(8.52 \pm 0.44) \times 10^{-4}$	1.938E-8			
	ϵ_0	$(5.42 \pm 0.19) \times 10^{-3}$	3.59E-9	3.43E-8		
	E_0 (keV)	393 ± 20	-7.95E-4	-2.72E-3	411	
Parameters			Value	Covariance Matrix		
D2	ϵ_c	$(8.29 \pm 0.43) \times 10^{-4}$	1.81E-9			
	ϵ_0	$(5.87 \pm 0.21) \times 10^{-3}$	3.88E-9	4.22E-8		
	E_0 (keV)	375 ± 19	-6.97E-4	-2.83E-3	350	
Parameters			Value	Covariance Matrix		
D3	ϵ_c	$(1.47 \pm 0.086) \times 10^{-3}$	7.38E-9			
	ϵ_0	$(1.46 \pm 0.09) \times 10^{-2}$	4.10E-8	8.13E-7		
	E_0 (keV)	297 ± 19	-1.37E-3	-1.45E-2	371	

Fig. 2: Measured half-life of (a) ^{95g}Tc and (b) ^{96g}Tc together with fit function (error bars in data points are smaller than symbol size).

The cross section σ is then extracted from N_γ and $Y(n)$ as below :

$$Y(n) = \frac{N_\gamma}{I_\gamma \varepsilon e^{-\lambda t_{\text{cool}}} (1 - e^{-\lambda t_{\text{count}}})}$$

$$\sigma = \frac{N_\gamma}{a N_t I_\gamma \varepsilon e^{-\lambda t_{\text{cool}}} (1 - e^{-\lambda t_{\text{count}}})} \frac{e}{X(n)} \quad (6)$$

3.2 Uncertainty analysis and correlation coefficients

The total uncertainty in the measured cross section is given by

$$\left(\frac{\Delta\sigma}{\sigma}\right)^2 = \left(\frac{\Delta N_\gamma}{N_\gamma}\right)^2 + \left(\frac{\Delta I_\gamma}{I_\gamma}\right)^2 + \left(\frac{\Delta a}{a}\right)^2 + \left(\frac{\Delta N_t}{N_t}\right)^2 + \left(\frac{\Delta \varepsilon}{\varepsilon}\right)^2 + \left(\frac{\Delta T_f}{T_f}\right)^2. \quad (7)$$

As mentioned earlier, targets are assumed to be uniform over the foil area ($\sim 1\text{cm}^2$) and the uncertainty estimated in target thickness is $\approx 0.6\%$, which is neglected

Table 3: Decay data taken from NNDC, together with the measured half-life from the present work for the measured channels.

Daughter nuclei	Reaction Channels	Decay Mode(%)	Q-value (MeV)	E_γ (keV)	I_γ (%)	$T_{1/2}$ (hrs)	$T_{1/2}^{expt}$ (hrs)
^{89g}Zr	$^{93}\text{Mo}(\text{p},\text{p}\alpha)$	EC $\beta+$ (100)	-4.359	909.15 \pm 0.15	99.04 \pm 0.03	78.41 \pm 0.12	84 \pm 5
	$^{94}\text{Mo}(\text{p},\text{d}\alpha)$		-11.812				
	$^{95}\text{Mo}(\text{p},\text{nd}\alpha)$		-19.181				
^{93g}Tc	$^{92}\text{Mo}(\text{p},\gamma)$	EC $\beta+$ (100)	4.087	1362.94 \pm 0.07	66.2 \pm 0.6	2.75 \pm 0.05	2.98 \pm 0.08
	$^{94}\text{Mo}(\text{p},2\text{n})$		-13.661				
	$^{95}\text{Mo}(\text{p},3\text{n})$		-21.031				
^{93m}Tc	$^{92}\text{Mo}(\text{p},\gamma)$	IT(77.4)	4.087	391.83 \pm 0.08	58.3 \pm 0.9	0.725 \pm 0.017	0.70 \pm 0.01
	$^{94}\text{Mo}(\text{p},2\text{n})$	EC $\beta+$ (22.6)	-14.415				
^{94g}Tc	$^{94}\text{Mo}(\text{p},\text{n})$	EC $\beta+$ (100)	-5.038	702.67 \pm 0.07	99.6 \pm 1.8	4.883 \pm 0.0167	4.8 \pm 0.1
	$^{95}\text{Mo}(\text{p},2\text{n})$		-12.407				
^{95g}Tc	$^{95}\text{Mo}(\text{p},\text{n})$	EC $\beta+$ (100)	-2.473	765.789 \pm 0.009	93.8 \pm 0.3	20 \pm 0.1	18.0 \pm 0.3
	$^{96}\text{Mo}(\text{p},2\text{n})$		-11.627				
	$^{97}\text{Mo}(\text{p},3\text{n})$		-18.448				
^{96g}Tc	$^{96}\text{Mo}(\text{p},\text{n})$	EC $\beta+$ (100)	-3.756	778.22 \pm 0.4	99.76 \pm 0.01	102.72 \pm 1.68	97 \pm 2
	$^{97}\text{Mo}(\text{p},2\text{n})$		-10.577				
	$^{98}\text{Mo}(\text{p},3\text{n})$		-19.219				
^{99m}Tc	$^{100}\text{Mo}(\text{p},2\text{n})$	IT(99.9963)	-8.574	140.511 \pm 0.001	89 \pm 4	6.0072 \pm 0.0009	6.1 \pm 0.1
	$^{100}\text{Mo}(\text{p},\text{pn})\rightarrow^{99}\text{Mo}\rightarrow^{99m}\text{Tc}$	EC $\beta+$ (0.0037)	-8.290				
	$^{100}\text{Mo}(\text{p},\text{d})\rightarrow^{99}\text{Mo}\rightarrow^{99m}\text{Tc}$		-6.607				
^{99}Mo	$^{100}\text{Mo}(\text{p},2\text{p})\rightarrow^{99}\text{Nb}\rightarrow^{99}\text{Mo}$	β -(100)	-11.140	739.5 \pm 0.017	12.2 \pm 0.2	65.924 \pm 0.006	63.1 \pm 0.1
	$^{100}\text{Mo}(\text{p},\text{pn})$		-8.290				
	$^{100}\text{Mo}(\text{p},\text{d})$		-6.607				

as it is much smaller compared to other factors. The uncertainty in isotopic fractions (a) and in proton flux (N_p) are also negligibly small. The uncertainty in the branching ratio (ΔI_γ) and timing factor T_f are treated as negligible whenever $\leq 0.1\%$ and taken into consideration otherwise.

Hence, the major contributions to the cross section uncertainty arise from N_γ (photopeak intensity) and the detector efficiency ϵ . The efficiency $\epsilon(E_\gamma(i))$ is interpolated using Eq. 2. The uncertainty $\Delta\epsilon(E_\gamma(i))$ in $\epsilon(E_\gamma(i))$ can be derived using the covariance matrix:

$$(\Delta\epsilon(E_\gamma(i)))^2 = \text{Cov}(\epsilon(E_\gamma(i)), \epsilon(E_\gamma(i))) \quad (8)$$

The covariance $\text{Cov}(\epsilon(E_i), \epsilon(E_j))$ is calculated as described in Ref [13]:

$$\begin{aligned} \text{Cov}(\epsilon(E_\gamma(i)), \epsilon(E_\gamma(j))) &= e^{-\frac{E_\gamma(i)+E_\gamma(j)}{E_0}} (\Delta\epsilon_0)^2 + \\ &\frac{\epsilon_0^2 E_\gamma(i) E_\gamma(j)}{E_0^4} e^{-\frac{E_\gamma(i)+E_\gamma(j)}{E_0}} (\Delta E_0)^2 + (\Delta\epsilon_c) + \\ &\epsilon_0 \frac{E_\gamma(i) + E_\gamma(j)}{E_0^2} e^{-\frac{E_\gamma(i)+E_\gamma(j)}{E_0}} \text{Cov}(\epsilon_0, E_0) + \\ &\left(e^{-\frac{E_\gamma(i)}{E_0}} + e^{-\frac{E_\gamma(j)}{E_0}} \right) \text{Cov}(\epsilon_0, \epsilon_c) + \\ &\frac{\epsilon_0}{E_0^2} \left(E_\gamma(i) e^{-\frac{E_\gamma(i)}{E_0}} + E_\gamma(j) e^{-\frac{E_\gamma(j)}{E_0}} \right) \text{Cov}(E_0, \epsilon_c). \end{aligned} \quad (9)$$

where E_0 , ϵ_0 and ϵ_c are fit parameters given in Table 2.

The covariance between cross sections σ_1 and σ_2 at proton energies E_1 and E_2 , respectively, is calculated us-

ing:

$$\text{Cov}(\sigma_1, \sigma_2) = \sum_k \left(\Delta x_k^{(1)} \cdot \text{Corr}(\Delta x_k^{(1)}, \Delta x_k^{(2)}) \cdot \Delta x_k^{(2)} \right), \quad (10)$$

where $\Delta x_k^{(1)}$ and $\Delta x_k^{(2)}$ are the fractional uncertainties of the k -th contributing term (see RHS of Eqn. 5) to the cross sections and $\text{Corr}(\Delta x_k^{(1)}, \Delta x_k^{(2)})$ represents the correlation between the k -th uncertainty components at two different proton energies.

The uncertainties in photopeak counts and number of target atoms present in the sample for different incident proton energies are not correlated and hence correlation coefficient between them is zero. Since the cross section measurement at different proton energies involves the same characteristic gamma ray E_γ , the corresponding $\epsilon(E_\gamma)$, I_γ and λ are same and consequently the fractional uncertainty in $\epsilon(E_\gamma(i))$ is identical at different proton energies. The correlation coefficient between cross sections at two different energies is calculated using the formula:

$$\text{Cor}(\sigma_1, \sigma_2) = \frac{\text{Cov}(\sigma_1, \sigma_2)}{(\Delta\sigma_1 \cdot \Delta\sigma_2)}. \quad (11)$$

4 Results and Discussion

Measured cross sections and corresponding total uncertainties for different reaction channels are tabulated in Tables 4 to 14. Fractional uncertainties of various parameters are also listed along with correlation coefficients. It should be mentioned that the accuracy of the current data is achieved through the systematic reduction of experimental uncertainties by using thin targets, precise beam current measurements, and corrections for isomer decay contributions (wherever possible). Further, a complete covariance evaluation has been performed for the first time for $\text{Mo}(\text{p},\text{x})$ reactions, providing cross section–cross section correlation coefficients that make the data more useful for comparisons with models and uncertainty propagation. To avoid the propagation of rounding off errors in the final cross section values and correlation coefficients, the uncertainty values in individual parameters are retained to two decimal places.

The present data are compared with the data available in the EXFOR library. From the observed $^{nat}\text{Mo}(\text{p},\text{x})$ cross section, $^{100}\text{Mo}(\text{p},\text{x})$ cross section is estimated employing appropriate scaling by the isotopic abundance of ^{100}Mo , for comparison with wider data sets.

4.1 Production of $^{89g+m}\text{Zr}$

The $^{89g+m}\text{Zr}$ is produced predominantly through $^{93}\text{Mo}(\text{p},\text{p}\alpha)$, $^{94}\text{Mo}(\text{p},\text{d}\alpha)$, and $^{95}\text{Mo}(\text{p},\text{nd}\alpha)$ reaction channels and the corresponding decay data together with Q -values are summarized in Table 3. The ^{89}Zr has an $\frac{1}{2}^-$ isomeric state at 587.8 keV with $T_{1/2} = 0.08$ hrs. Due to relatively short half-life, the production cross section of this

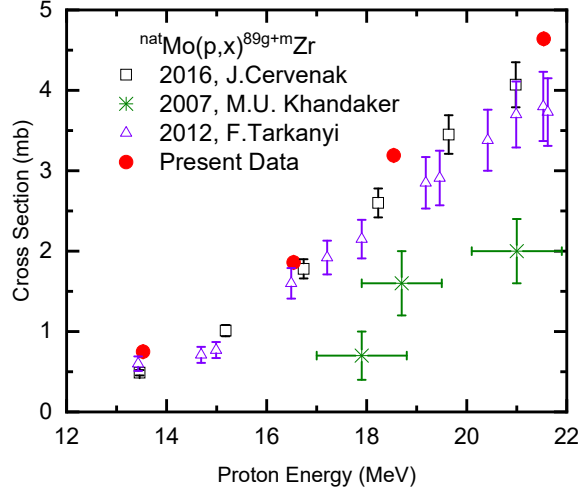
^{89m}Zr state could not be measured in the present experiment. This state has two decay branches: electron capture (EC) to ^{89}Y , branching ratio of 6.23% and M4 transition (IT) ^{89}Zr ground state ($\frac{1}{2}^+$), branching ratio of 93.77%. While the latter (IT) is included in sum total of measured $^{89(g+m)}\text{Zr}$, the contribution of the former could not be assessed. The measured cross sections and the corresponding correlation coefficients for various proton energies are summarized in Table 4. Figure 3 compares the present data with measurements reported in Refs. [7], [14] and [15]. As can be seen in the figure, the previous reported data are scattered with large uncertainties (especially from [7]) and discrepancies are observed between the measured cross sections. The large uncertainties in the incident beam energy in [7] may be due to the use of thick targets. On the other hand, the present experiment used thin, high-purity molybdenum foils and proton beam with energy resolution better than 0.1 MeV, thereby yielding more accurate excitation function. Present data is consistent with that of [14] and [15], and plays an important role in resolving the discrepancy in previously reported data. Additionally, covariance analysis is carried out for the first time for this reaction, making these results more valuable for model evaluation and yield optimization than older datasets without uncertainty correlations. The observed increasing trend of σ with E also highlights the importance of measurements at higher proton energies to optimize the $^{89g+m}\text{Zr}$ production.

4.2 Production of ^{93}Tc

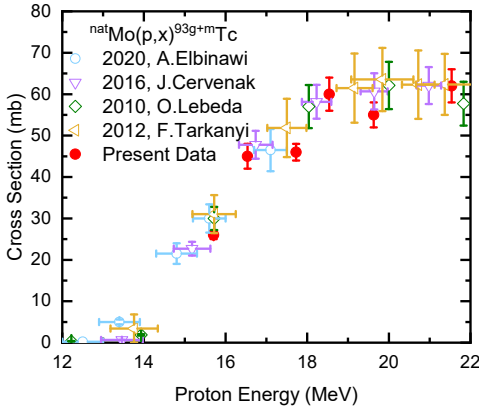
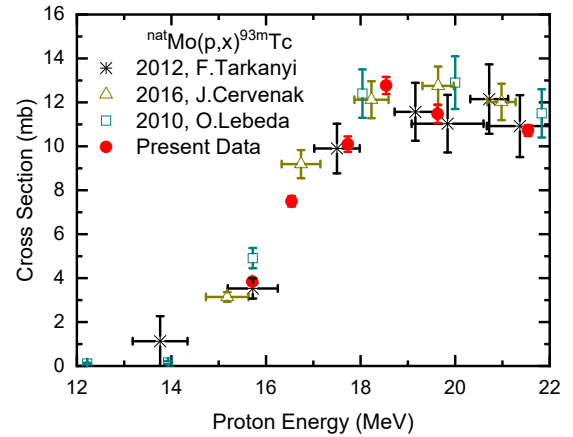
The ^{93}Tc can be produced either in the ground state or in the isomeric state via $^{92}\text{Mo}(\text{p},\gamma)$, $^{94}\text{Mo}(\text{p},2\text{n})$ and $^{95}\text{Mo}(\text{p},3\text{n})$ reactions as listed in Table 3. However, $^{92}\text{Mo}(\text{p},\gamma)$ cross sections are very small and due to high Q value contribution from $^{95}\text{Mo}(\text{p},3\text{n})$ is relevant ($\sim 10\%$) only at the highest incident energy. The isomeric state ^{93m}Tc ($1/2^-$, $T_{1/2} = 0.725$ hrs) de-excites either via an M4 gamma transition to ^{93g}Tc ($f \sim 77.4\%$) or via electron capture to ^{93}Mo ($\sim 22.6\%$). Given the comparable half-lives of ^{93m}Tc and ^{93g}Tc , the measured yield of 1362 keV gamma ray (from the decay of ^{93g}Tc) has contributions from the directly produced ground state (^{93g}Tc) and the isomeric decay ^{93m}Tc . Most previous studies have reported combined $^{93g+m}\text{Tc}$ yield, making it difficult to assess the independent ground state production in ^{93g}Tc . In a couple of cases e.g. [14], [15] the ^{93g}Tc cross section is estimated either by neglecting or approximating decay corrections. In the present work, the cross section for the direct production of ^{93g}Tc is extracted by proper subtraction of the ^{93m}Tc isomer decay contribution from the cumulative yield $^{93g+m}\text{Tc}$.

4.2.1 Production of $^{93g+m}\text{Tc}$

The N_{1362} , total observed photopeak counts for 1362 keV gamma ray during counting, can be expressed as

Fig. 3: Excitation function for production of $^{89g+m}\text{Zr}$.Table 4: cross sections for $^{nat}\text{Mo}(p,x)^{89g+m}\text{Zr}$ reaction together with fractional uncertainty in parameters and correlation coefficients between E_p and σ .

E_p (MeV)	σ (mb)	$\Delta\epsilon$ (%)	ΔN_t (%)	ΔN_γ (%)	Total Uncertainty (%)	Correlation coefficients			
21.54	4.6 ± 0.1	1.38	0.52	2.48	2.88	1			
18.54	3.2 ± 0.1	1.38	0.64	3.67	3.97	0.17	1		
16.54	1.9 ± 0.2	1.38	0.59	8.07	8.21	0.08	0.06	1	
13.53	0.75 ± 0.14	2.35	0.53	18.93	19.08	0.06	0.04	0.02	1

Fig. 4: Excitation function of $^{nat}\text{Mo}(p,x)^{93g+m}\text{Tc}$ reaction.Fig. 5: Excitation function of $^{nat}\text{Mo}(p,x)^{93m}\text{Tc}$ reaction.

$$N_{1362} = \varepsilon I_\gamma \int_{t_1}^{t_2} \frac{d}{dt} [Y_g^{\text{direct}}(t) + Y_{m \rightarrow g}(t)] dt \quad (12)$$

where Y_g^{direct} and $Y_{m \rightarrow g}$ represent the yield of ^{93g}Tc produced directly and from the decay of ^{93m}Tc , respectively. The total $^{93g+m}\text{Tc}$ cross section values obtained from net

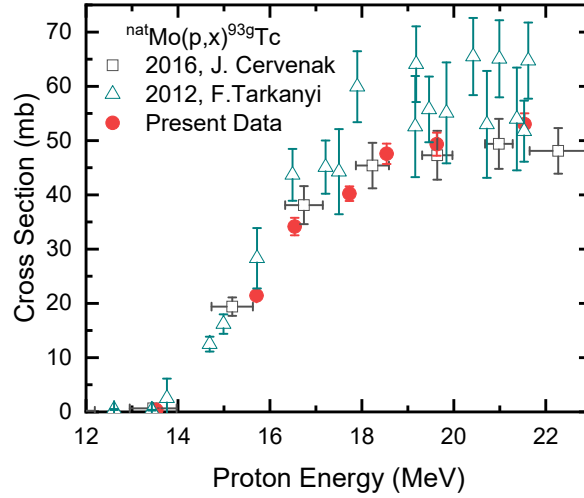
yield of 1362 keV gamma ray are given in Table 5 together with the corresponding correlation coefficients for different incident proton energies. The data are plotted in Fig. 4. It can be seen from the figure that the cross sections for the $^{nat}\text{Mo}(p,x)^{93g+m}\text{Tc}$ reaction, increase from about 12 to 18 MeV and are nearly constant thereafter. The present data is in good agreement with the previously reported measurements in Refs. [14]-[18]. It should be emphasized

Table 5: cross sections for $^{nat}\text{Mo}(\text{p},\text{x})^{93g+m}\text{Tc}$ reaction together with fractional uncertainty in parameters and correlation coefficients between E_p and σ .

E_p (MeV)	σ (mb)	ΔT_f (%)	$\Delta\epsilon$ (%)	ΔI_γ (%)	ΔN_t (%)	ΔN_γ (%)	Total Uncertainty (%)	Correlation coefficients						
21.54	53±2	1.92	2.21	0.91	0.52	1.57	3.48	1						
19.63	42±2	2.06	2.30	0.91	0.44	1.40	3.54	0.39	1					
18.54	57±2	0.94	2.21	0.91	0.64	2.31	3.51	0.61	0.22	1				
17.73	34±1	0.90	2.30	0.91	0.44	1.28	2.96	0.25	0.76	0.16	1			
16.54	37±2	1.30	2.21	0.91	0.59	3.48	4.46	0.53	0.22	0.44	0.15	1		
15.71	23±1	0.02	2.30	0.91	0.46	2.07	3.26	0.08	0.53	0.07	0.64	0.06	1	

Table 6: cross sections for $^{nat}\text{Mo}(\text{p},\text{x})^{93m}\text{Tc}$ reaction together with fractional uncertainty in parameters and correlation coefficients between E_p and σ .

E_p (MeV)	σ (mb)	ΔT_f (%)	$\Delta\epsilon$ (%)	ΔI_γ (%)	ΔN_t (%)	ΔN_γ (%)	Total Uncertainty (%)	Correlation coefficients						
21.54	10.7±0.2	0.68	1.40	1.54	0.52	0.52	2.31	1						
19.63	11.4±0.4	2.34	1.49	1.54	0.44	1.77	3.66	0.47	1					
18.54	12.8±0.4	1.64	1.40	1.54	0.64	1.39	3.06	0.77	0.56	1				
17.73	10.1±0.4	1.84	1.49	1.54	0.44	1.97	3.47	0.45	0.70	0.51	1			
16.54	7.5±0.2	0.04	1.40	1.54	0.59	2.38	3.22	0.59	0.21	0.45	0.22	1		
15.71	3.8±0.2	1.91	1.49	1.54	0.46	2.69	3.96	0.40	0.63	0.46	0.59	0.19	1	

Fig. 6: Excitation function for production of ^{93g}Tc .

that the reduced uncertainties in the present data provide a more reliable evaluation of the $^{93g+m}\text{Tc}$ production channel.

4.2.2 Production of ^{93m}Tc :

The ^{93m}Tc isomer is important for medical isotope studies because its decay directly contributes to the production of ^{93g}Tc . The measured cross section values along with the correlation coefficients for various incident proton energies are listed in Table 6. The comparison of the present data with the earlier data reported in Refs. [14]-[16] is shown in Figure 5. Present measurements show

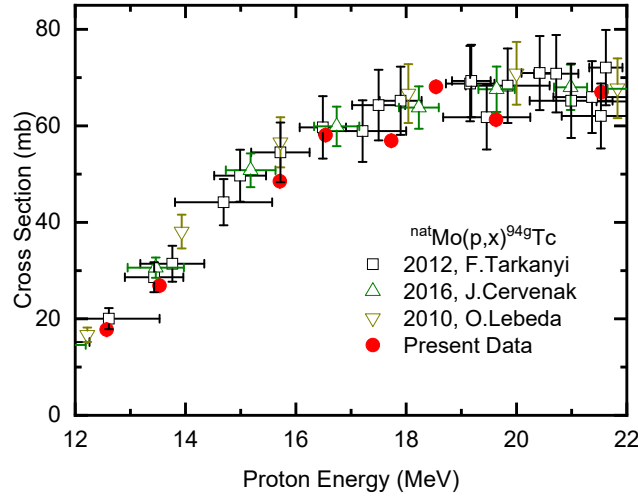
overall agreement with the reported data, while a significant improvement in the in data quality is evident since energy uncertainties are considerably reduced with use of thin targets.

4.2.3 Production of ^{93g}Tc

The determination of the direct ^{93g}Tc production cross section represents one of the key strengths of the present work. The second term $Y_{m\rightarrow g}$ in equation [12] is computed using the $\sigma(^{93m}\text{Tc})$ obtained in subsection 4.2.2. Employing the procedure described in section 3.1, yield of ^{93m}Tc at the end of the i^{th} interval, $Y_{93m}(i)$, is given by

Table 7: cross sections for $^{nat}\text{Mo}(\text{p},\text{x})^{93g}\text{Tc}$ reaction together with fractional uncertainty in parameters and correlation coefficients between E_p and σ .

E_p (MeV)	$\sigma(\text{mb})$	ΔT_f (%)	$\Delta\epsilon$ (%)	ΔI_γ (%)	ΔN_t (%)	ΔN_γ (%)	Total Uncertainty (%)	Correlation coefficients							
21.54	53±2	1.92	2.21	0.91	0.52	2.13	3.76	1							
19.63	49±2	2.06	2.30	0.91	0.44	2.82	4.30	0.30	1						
18.54	48±2	0.94	2.21	0.91	0.64	2.93	3.94	0.51	0.16	1					
17.73	40±1	0.90	2.30	0.91	0.44	2.02	3.35	0.20	0.55	0.13	1				
16.54	34±2	1.30	2.21	0.91	0.59	3.80	4.71	0.46	0.17	0.37	0.13	1			
15.71	21±1	0.02	2.30	0.91	0.46	1.78	3.08	0.07	0.46	0.07	0.59	0.06	1		
13.53	0.34±0.06	0.47	2.30	0.91	0.53	17.07	17.27	0.03	0.10	0.02	0.11	0.02	0.12	1	

Fig. 7: Excitation function for production of ^{94g}Tc .Table 8: cross sections for $^{nat}\text{Mo}(\text{p},\text{x})^{94g}\text{Tc}$ reaction together with fractional uncertainty in parameters and correlation coefficients between E_p and σ .

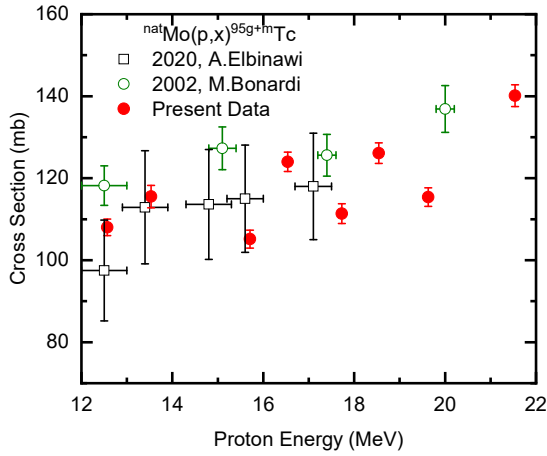
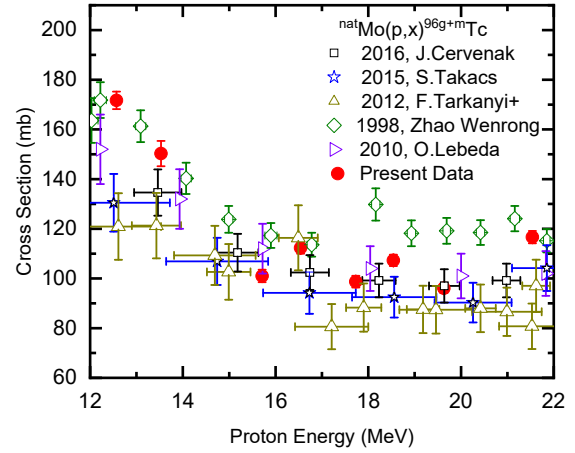
E_p (MeV)	$\sigma(\text{mb})$	ΔT_f (%)	$\Delta\epsilon$ (%)	ΔI_γ (%)	ΔN_t (%)	ΔN_γ (%)	Total Uncertainty (%)	Correlation coefficients								
21.54	67.0±0.3	0.27	1.64	1.81	0.52	3.24	4.09	1								
19.63	61.3±0.2	0.23	1.73	1.81	0.44	1.22	2.82	0.29	1							
18.54	68.1±0.2	0.25	1.64	1.81	0.64	2.22	3.37	0.44	0.35	1						
17.73	56.9±0.2	0.24	1.73	1.81	0.44	0.93	2.72	0.30	0.82	0.36	1					
16.54	58.1±0.2	0.29	1.64	1.81	0.59	2.89	3.84	0.38	0.31	0.47	0.32	1				
15.71	48.5±0.1	0.14	1.73	1.81	0.46	0.83	2.68	0.30	0.83	0.37	0.86	0.32	1			
13.53	26.9±0.1	0.10	1.73	1.81	0.53	1.18	2.82	0.29	0.79	0.35	0.82	0.30	0.83	1		
12.57	17.8±0.1	0.25	1.64	1.81	0.55	2.26	3.38	0.43	0.35	0.53	0.36	0.46	0.36	0.35	1	

$$Y_{93m}(i) = Y_{93m}(i-1) + K_m dq(i) - \lambda_m Y_{93m}(i-1) dt(i) \quad (13)$$

where K_m is the production rate of ^{93m}Tc per unit charge and λ_m is the decay constant. Given the fraction f feeding the ground state from the isomer decay and the decay constant for the ground state λ_g , the yield of the ^{93g}Tc from the isomer decay at the end of the i^{th} interval can be expressed as

$$Y_{m \rightarrow g}(i) = Y_{m \rightarrow g}(i-1) + f \lambda_m Y_{93m}(i-1) dt(i) - \lambda_g Y_{m \rightarrow g}(i-1) dt(i), \quad (14)$$

Thus, $Y_{m \rightarrow g}$ can be computed at the end of the irradiation. Further, the $Y_{m \rightarrow g}$ is computed during the cooling time and the counting time following the same procedure, by setting the production rate of ^{93m}Tc to zero. The counting period t_{count} is divided into J_{cnt} intervals of duration dt each and total number of ground-state decays (D_g) are

Fig. 8: Excitation function for production of $^{95g+m}\text{Tc}$.Fig. 9: Excitation function for production of $^{96g+m}\text{Tc}$.Table 9: cross sections for $^{nat}\text{Mo}(p,x)^{95g+m}\text{Tc}$ reaction together with fractional uncertainty in parameters and correlation coefficients between E_p and σ .

E_p (MeV)	σ (mb)	ΔT_f (%)	$\Delta \epsilon$ (%)	ΔI_γ (%)	ΔN_t (%)	ΔN_γ (%)	Total Uncertainty (%)	Correlation coefficients									
21.54	140 ± 3	0.20	1.58	0.32	0.52	0.85	1.91	1									
19.63	115 ± 3	0.10	1.68	0.32	0.44	0.84	1.95	0.03	1								
18.54	126 ± 3	0.18	1.58	0.32	0.64	0.93	1.98	0.70	0.03	1							
17.73	111 ± 2	0.19	1.54	0.32	0.44	1.40	2.16	0.03	0.64	0.03	1						
16.54	124 ± 2	0.18	1.58	0.32	0.59	0.79	1.90	0.73	0.03	0.70	0.03	1					
15.71	105 ± 2	0.23	1.68	0.32	0.46	1.10	2.09	0.04	0.72	0.03	0.60	0.04	1				
13.53	116 ± 3	0.23	1.54	0.32	0.53	1.65	2.36	0.03	0.59	0.03	0.50	0.03	0.56	1			
12.57	108 ± 2	0.24	1.58	0.32	0.55	0.75	1.88	0.74	0.03	0.71	0.04	0.74	0.04	0.04	1		

computed as

$$D_g = \sum_{j=1}^{J_{\text{CNT}}} \lambda_g Y_{m \rightarrow g}(j-1) dt(j), \quad (15)$$

The contribution from $m \rightarrow g$ feeding to the photopeak yield of 1362 keV is given by

$$N_{1362}(m \rightarrow g) = \varepsilon I_\gamma D_g, \quad (16)$$

The direct ground-state contribution to 1362 photopeak counts is obtained as

$$N_{1362}^{\text{direct}} = N_{1362} - N_{1362}(m \rightarrow g), \quad (17)$$

Again employing the same procedure described in section 3.1, the direct production cross section of ^{93g}Tc , σ_g , is extracted. This step-by-step calculation of production and decay of both ^{93m}Tc and ^{93g}Tc throughout irradiation, cooling, and counting, properly accounts for beam fluctuations and decay corrections, yielding accurate values of $\sigma(^{93g}\text{Tc})$.

The extracted $\sigma(^{93g}\text{Tc})$ values along with their correlation coefficients at different proton energies are listed in Table 7. and plotted in Figure 6. As is evident from the

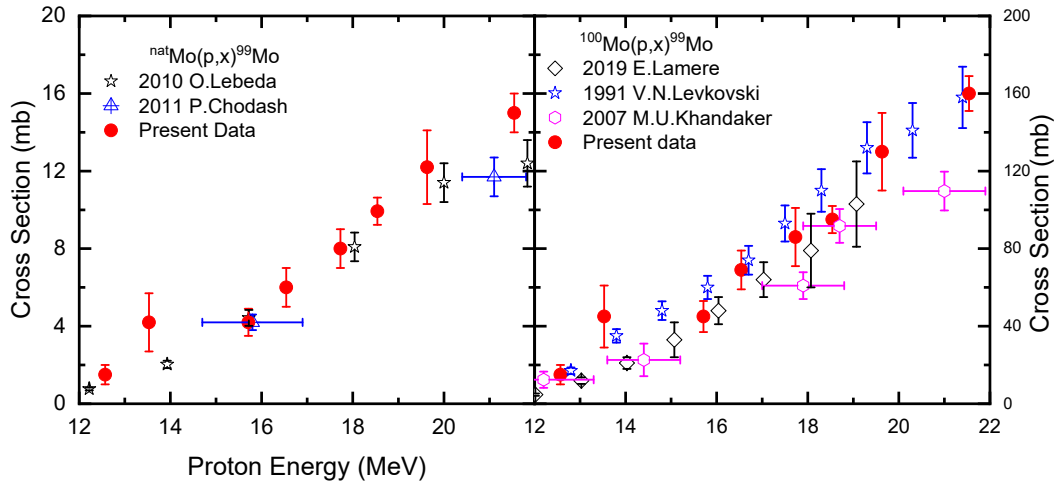
Figure the cross section increases rapidly upto 18 MeV and is nearly constant at higher energies. It should be mentioned that the lowest beam energy of 13.53 MeV in the present experiment is significantly lower than the Q-value of the $^{94}\text{Mo}(p,2n)^{93m}\text{Tc}$ reaction and hence the observed cross section at this energy corresponds only to the production of ^{93g}Tc . The data of [14] and [15] are also shown for a comparison, although in these works the decay corrections are not properly incorporated. Measurements at higher energies are desirable to understand the saturation value of ^{93g}Tc production.

4.3 Production of ^{94g}Tc :

The ^{94g}Tc production occurs predominantly through the $^{95}\text{Mo}(p,2n)$ and $^{94}\text{Mo}(p,n)$ channels as listed in Table 3. The measured cross section values of ^{94g}Tc production are listed in Table 8, together with the corresponding correlation coefficients. Figure 7 shows a comparison of the present excitation function with previously reported measurements. Measurements reported in Refs. [17–21] show a similar general trend, but have large uncertainties as well as large spread and hence have not been included in the comparison. The present data shows an overall agreement

Table 10: cross sections for $^{nat}\text{Mo}(\text{p},\text{x})^{96g+m}\text{Tc}$ reaction together with fractional uncertainty in parameters and correlation coefficients between E_p and σ .

E_p (MeV)	σ (mb)	ΔT_f (%)	$\Delta\epsilon$ (%)	ΔN_i (%)	ΔN_γ (%)	Total Uncertainty (%)	Correlation coefficients										
21.54	117±3	1.13	1.57	0.52	0.74	2.13	1										
19.63	96±2	0.58	1.66	0.44	0.85	2.00	0.15	1									
18.54	107±2	1.04	1.57	0.64	0.81	2.15	0.79	0.14	1								
17.73	99±2	1.06	1.53	0.44	1.44	2.40	0.23	0.66	0.21	1							
16.54	112±2	0.94	1.57	0.59	0.82	2.09	0.79	0.13	0.77	0.20	1						
15.71	101±3	1.28	1.66	0.46	1.28	2.50	0.27	0.70	0.25	0.65	0.23	1					
13.53	150±5	0.92	2.74	0.53	1.71	3.40	0.14	0.75	0.13	0.63	0.12	0.67	1				
12.57	172±4	0.88	1.57	0.55	0.85	2.06	0.78	0.12	0.76	0.19	0.76	0.22	0.12	1			

Fig. 10: Excitation function for (a) $^{nat}\text{Mo}(\text{p},\text{x})^{99}\text{Mo}$ and (b) $^{100}\text{Mo}(\text{p},\text{x})^{99}\text{Mo}$ reactions.

with the excitation function as that of [14–16], with much smaller uncertainties.

4.4 Production of $^{95g+m}\text{Tc}$:

In the $^{nat}\text{Mo}(\text{p},\text{x})$ reactions, ^{95}Tc can be produced either in the ground state or in the isomeric state ^{95m}Tc ($1/2^-$). The isomeric state decays to the ground state either by a gamma transition $1/2^- \rightarrow 9/2^+$ (branching ratio of 3.88%), or by electron capture to ^{95}Mo (branching ratio 96.12%). Due to the long half-life of ^{95m}Tc ($T_{1/2} = 1464$ hrs), its production cross section could not be measured directly. However, it contributes to the measured yield of 765.8 keV gamma ray, observed in the decay of ^{95g}Tc . Hence, the present data represent the combined $^{95(g+m)}\text{Tc}$ production. Figure 8 compares the measured excitation function of $^{nat}\text{Mo}(\text{p},\text{x})^{95g+m}\text{Tc}$ with previously reported data. It should be pointed out that in the energy window of interest (12–22 MeV), measurements of Bonardi et al. [21] have very sparse data points, while more recent data [17] are limited to $E_p < 17$ MeV and have large uncertainties (both in E and σ). The present data indicates

that cross section is nearly constant upto 20 MeV. Further measurements are needed at higher energy as about 20% increase is observed at the highest energy. The cross section values along with respective correlation coefficients are summarized in Table 9.

4.5 Production of $^{96g+m}\text{Tc}$:

The production of ^{96}Tc occurs primarily through the $^{96}\text{Mo}(\text{p},\text{n})$, $^{97}\text{Mo}(\text{p},2\text{n})$, and $^{98}\text{Mo}(\text{p},3\text{n})$ reaction channels, as listed in Table 3. In the case of ^{96}Tc also, the measured ground state data has contribution from the isomeric state ^{96m}Tc (4^+ , $T_{1/2} = 0.86$ hrs), which could not be extracted separately. The isomer decays predominantly via an M3 gamma transition to the ground state (IT 98%), while a small fraction (2%) decays to ^{96}Mo following an EC. Consequently, the measured cross sections ^{96}Tc represent the combined production of $^{96(g+m)}\text{Tc}$. The measured data for various proton energies is tabulated in Table 10 together with the corresponding correlation coefficients. Figure 9 shows the excitation function of the $^{96g+m}\text{Tc}$

Table 11: cross sections for $^{nat}\text{Mo}(\text{p},\text{x})^{99}\text{Mo}$ reaction together with fractional uncertainty in parameters and correlation coefficients between E_p and σ .

E_p (MeV)	σ (mb)	$\Delta\epsilon$ (%)	ΔI_γ (%)	ΔN_t (%)	ΔN_γ (%)	Total Uncertainty (%)	Correlation coefficients							
21.54	15±1	1.61	1.64	0.52	5.10	5.62	1							
19.63	12.2±1.9	1.70	1.64	0.44	15.32	15.50	0.03	1						
18.54	9.3±0.7	1.61	1.64	0.64	7.07	7.46	0.13	0.02	1					
17.73	8±1	1.57	1.64	0.44	17.77	17.92	0.03	0.02	0.02	1				
16.54	6±1	1.61	1.64	0.59	14.53	14.72	0.06	0.01	0.05	0.01	1			
15.71	4.2±0.7	1.70	1.64	0.46	16.55	16.73	0.03	0.02	0.02	0.02	0.01	1		
13.53	4.2±1.5	2.84	1.64	0.53	36.19	36.35	0.01	0.01	0.01	0.01	0.01	0.01	0.01	1
12.57	1.5±0.5	1.61	1.64	0.55	32.84	32.92	0.03	0.01	0.02	0.005	0.01	0.005	0.002	1

Table 12: cross sections for $^{100}\text{Mo}(\text{p},\text{x})^{99}\text{Mo}$ reaction together with fractional uncertainty in parameters and correlation coefficients between E_p and σ .

E_p (MeV)	σ (mb)	$\Delta\epsilon$ (%)	ΔI_γ (%)	Δa (%)	ΔN_t (%)	ΔN_γ (%)	Total Uncertainty (%)	Correlation coefficients							
21.54	160±9	1.61	1.64	0.67	0.52	5.10	5.66	1							
19.63	130±20	1.70	1.64	0.67	0.44	15.32	15.52	0.04	1						
18.54	95±7	1.61	1.64	0.67	0.64	7.07	7.49	0.14	0.03	1					
17.73	86±15	1.57	1.64	0.67	0.44	17.77	17.93	0.03	0.02	0.02	1				
16.54	69±10	1.61	1.64	0.67	0.59	14.53	14.73	0.07	0.01	0.05	0.01	1			
15.71	45±8	1.70	1.64	0.67	0.46	16.55	16.74	0.03	0.02	0.02	0.02	0.01	1		
13.53	45±16	2.84	1.64	0.67	0.53	36.19	36.35	0.02	0.01	0.01	0.01	0.01	0.01	1	
12.57	15±5	1.61	1.64	0.67	0.55	32.84	32.93	0.03	0.01	0.02	0.01	0.01	0.01	0.003	1

production. The present data shows that the cross section decreases from about 12 to 16 MeV and is nearly constant thereafter, which is similar to earlier measurements ([14]–[17], [21]–[23]). The improved precision and consequently a better quality of the data is evident from the figure.

4.6 Production of ^{99}Mo :

The main contributing channels to ^{99}Mo production are summarized in Table 3. Measured cross sections for the $^{nat}\text{Mo}(\text{p},\text{x})^{99}\text{Mo}$ are listed in Table 11 together with correlation coefficients and are plotted in Figures 10 (a). The derived cross section for and $^{100}\text{Mo}(\text{p},\text{x})^{99}\text{Mo}$ reaction from the above data are given in Table 12 and are plotted in in Figure 10(b). As can be seen from the Figure, the present data are in good agreement with prior studies [7, 16, 24–26]. For ^{99}Mo , the uncertainties in the present measurements are comparable to those reported in previous works. However, it should be pointed out that Levkovski et al. [26] did not report the proton beam energy spread.

4.7 Production of ^{99m}Tc :

The ^{99m}Tc can be produced via $^{100}\text{Mo}(\text{p},\text{x})$ reactions as detailed in Table 3. The contribution from $^{98}\text{Mo}(\text{p},\gamma)$ channel is also suggested by [7]. The extraction of production cross section ^{99m}Tc is complicated due the contribution from beta decay of ^{99}Mo . The ^{99}Mo predominantly

decays to the ^{99m}Tc ($f \sim 87.9\%$) [27], a small fraction (5.1%) [23] decays to the 140.5 keV state in ^{99}Tc and remaining fraction decays to the ground state of ^{99}Tc . Hence, the observed photopeak yield of 140.5 keV line, N_{140} needs to be corrected for the beta decay contribution of ^{99}Mo .

$$N_{140}^m = N_{140}^{obs} - N_{140}^{Mo}$$

Similar to Eq. 12, N_{140}^m can be written as

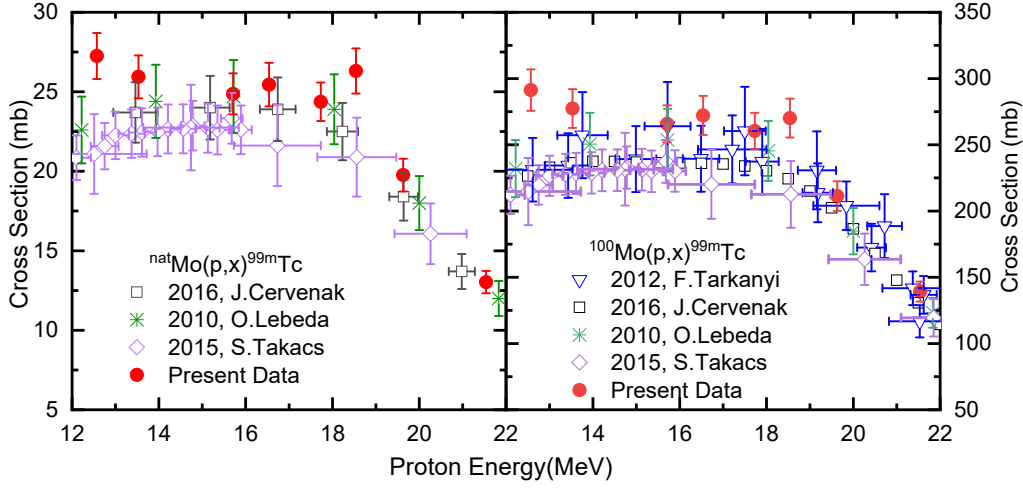
$$N_{140}^m = \varepsilon_{140} I_{\gamma 1} \int_{t_1}^{t_2} \frac{d}{dt} [Y_{mTc}^{direct}(t) + Y_{Mo \rightarrow m}(t)] dt \quad (18)$$

where ε_{140} and $I_{\gamma 1}$ are photopeak efficiency and branching ratio of 140 keV gamma ray, respectively. The ^{99m}Tc production cross section is obtained using the similar methodology described in Sections 4.2.3. The yields of ^{99}Mo and ^{99m}Tc from ^{99}Mo decay at the end of the i^{th} time interval, $Y_{Mo}(i)$ and $Y_{Mo \rightarrow m}(i)$, respectively, can be written as

$$Y_{Mo}(i) = Y_{Mo}(i-1) + P_{99Mo}(i) - \lambda_1 Y_{Mo}(i-1) dt(i) \quad (19)$$

$$Y_{Mo \rightarrow m}(i) = Y_{Mo \rightarrow m}(i-1) + 0.879\lambda_1 Y_{Mo}(i-1) dt(i) - \lambda_2 Y_{Mo \rightarrow m}(i-1) dt(i) \quad (20)$$

where λ_1 and λ_2 are decay constants of ^{99}Mo and ^{99m}Tc , respectively and $P_{99Mo}(i)$ is the production rate given by eq. 5. Although $\lambda_1 \ll \lambda_2$, interval wise computation process has been adopted for better precision. The contribution from ^{99}Mo to ^{99m}Tc decay in the observed photopeak

Fig. 11: Excitation function for (a) $^{nat}\text{Mo}(p,x)^{99m}\text{Tc}$ and (b) $^{100}\text{Mo}(p,x)^{99m}\text{Tc}$ reactions.Table 13: cross sections for $^{nat}\text{Mo}(p,x)^{99m}\text{Tc}$ reaction together with fractional uncertainty in parameters and correlation coefficients between E_p and σ .

E_p (MeV)	σ (mb)	$\Delta\epsilon$ (%)	ΔI_γ (%)	ΔN_t (%)	ΔN_γ (%)	Total Uncertainty (%)	Correlation coefficients									
21.54	13±1	2.16	4.49	0.52	1.98	5.39	1									
19.63	20±1	2.20	4.49	0.44	1.46	5.23	0.72	1								
18.54	26±1	2.16	4.49	0.64	1.94	5.39	0.86	0.72	1							
17.73	24±1	1.57	4.49	0.44	1.30	4.95	0.76	0.91	0.76	1						
16.54	25±1	2.16	4.49	0.59	1.96	5.39	0.86	0.72	0.86	0.76	1					
15.71	25±1	2.20	4.49	0.46	1.30	5.19	0.72	0.92	0.72	0.92	0.72	1				
13.53	26±1	2.20	4.49	0.53	1.38	5.22	0.72	0.92	0.72	0.91	0.72	0.92	1			
12.57	27±2	2.16	4.49	0.55	1.79	5.33	0.87	0.72	0.87	0.77	0.87	0.73	0.73	1		

Table 14: cross sections for $^{100}\text{Mo}(p,x)^{99m}\text{Tc}$ reaction together with fractional uncertainty in parameters and correlation coefficients between E_p and σ .

E_p (MeV)	σ (mb)	$\Delta\epsilon$ (%)	ΔI_γ (%)	Δa (%)	ΔN_t (%)	ΔN_γ (%)	Total Uncertainty (%)	Correlation coefficients								
21.54	139±8	2.16	4.49	0.67	0.52	1.98	5.43	1								
19.63	211±11	2.20	4.49	0.67	0.44	1.46	5.27	0.72	1							
18.54	270±15	2.16	4.49	0.67	0.64	1.94	5.43	0.86	0.72	1						
17.73	260±14	2.20	4.49	0.67	0.44	1.30	5.23	0.73	0.92	0.73	1					
16.54	272±15	2.16	4.49	0.67	0.59	1.96	5.43	0.86	0.72	0.86	0.73	1				
15.71	266±14	2.20	4.49	0.67	0.46	1.30	5.23	0.73	0.92	0.73	0.93	0.73	1			
13.53	277±15	2.20	4.49	0.67	0.53	1.38	5.26	0.72	0.92	0.72	0.93	0.72	0.93	1		
12.57	291±16	2.16	4.49	0.67	0.55	1.79	5.37	0.87	0.73	0.87	0.73	0.87	0.73	0.73	1	

yield of 140 keV, $N_{140}^{Mo \rightarrow m}$, is computed using the cross section $\sigma(^{99}\text{Mo})$ obtained in Section 4.6. Then the contribution to the photopeak counts from the direct isomer production ^{99m}Tc is obtained as

$$N_{140}^{m-direct} = N_{140}^m - N_{140}^{Mo \rightarrow m} \quad (21)$$

The direct isomer production cross section $\sigma(^{99m}\text{Tc})$ is extracted from $N_{140}^{m-direct}$.

In Fig. 11 (a) and (b), the measured excitation functions of the $^{nat,100}\text{Mo}(p,x)^{99m}\text{Tc}$ reactions are compared with previously reported data [14–16,23]. The observed trend in present cross sections is consistent with the reported values, namely, constant up to 18 MeV and rapid decrease thereafter. However, the absolute values of the measured cross section is higher at $E < 14$ MeV. It should be mentioned that the data for the $^{nat}\text{Mo}(p,x)^{99m}\text{Tc}$ re-

action reported in [7] and [28] correspond only to the reaction $^{100}\text{Mo}(p,2n)^{99m}\text{Tc}$ and therefore are not directly comparable with our data. The measured cross sections along with the corresponding correlation coefficients are listed in Tables 13 and 14, respectively, for different incident proton energies.

5 Conclusion

This study reports new measurements of $^{nat}\text{Mo}(p,x)$ and $^{100}\text{Mo}(p,x)$ reaction cross sections in the proton energy range of 12 to 22 MeV with substantially reduced uncertainties, as compared to previously reported data. In the present work, the enhanced precision was achieved through usage of thin targets, precise beam current measurements, and systematic corrections for isomeric contributions. For proton induced reactions on molybdenum, covariance information is reported for the first time and provides correlation coefficients between the measured cross sections. Consequently, the present measurements are important not only for reduced uncertainties but also for more precisely quantified error propagation, thereby providing greater confidence in their application to nuclear data evaluation. Hence, these results contribute to strengthening international databases such as EXFOR and serve as reliable benchmarks for widely used nuclear reaction codes including TALYS, EMPIRE, and ALICE. Equally important, the data also hold direct relevance for medical isotope production. The measured excitation functions for ^{99m}Tc and ^{99}Mo support their established use in SPECT imaging and generator systems, while ^{96g}Tc and ^{95g}Tc show promise as potential alternatives or tracers. Additional isotopes such as ^{94g}Tc , ^{93g}Tc and ^{89g}Tc are of growing interest in PET imaging and targeted oncology. By combining reduced uncertainties with clinically relevant outcomes, this work strengthens the bridge between nuclear data research and healthcare applications, ensuring lasting impact on both nuclear science and medical diagnostics.

6 Acknowledgement

We thank the PLF staff for the smooth accelerator operation, Mr. R.D. Turbhekar and Mr. N.C. Kamble for the target preparations, Mr. Nishant Jangid and Mr. Kiran Divekar for assistance during the experiment and N.Otsuka for his guidance during analysis. The financial support from the Science and Engineering Research Board, Government of India (GoI)(Sanction No. EEQ/2022/000545, dated 17.02.2023), from the Institution of Eminence (IoE), Banaras Hindu University (Grant No. 6031-B) and from the Department of Atomic Energy (GoI), under Project No. RTI4002 is gratefully acknowledged. One of the authors, SB, acknowledges the financial support provided by the University Grants Commission (UGC), New Delhi, India, under the Junior Research Fellowship (JRF) scheme [fellowship award reference number:231610089402].

References

1. Siddharth Parashari, S. Mukherjee, S.V. Suryanarayana, B.K. Nayak, Rajnikant Makwana, N.L. Singh, H. Naik, Systematic analysis of the neutron-induced reaction cross sections for Mo nat isotopes within 10–20 MeV, *Phys. Rev. C* **99**, 4, 044602 (2019).
2. Wang, Yiwei; Chen, Daiyuan; dos Santos Augusto, Ricardo; Liang, Jixin; Qin, Zhi; Liu, Juntao; Liu, Zhiyi. Production review of accelerator-based medical isotopes. *Molecules* **2022**, 27(16), 5294. MDPI.
3. I. Mazumdar, M. Dhibar, S.P. Weppner, G.A. Kumar, A.K. Rhine Kumar, S.M. Patel, P.B. Chavan, C.D. Bagdia, L.C. Tribedi, Studies in Nuclear Structure and Big Bang Nucleosynthesis Using Proton Beams, *Acta Phys. Pol. B* **50**, 3, 377 (2019).
4. M.G. Lobok, A.V. Brantov, V.Yu. Bychenkov, Laser-based photonuclear production of medical isotopes and nuclear waste transmutation, *Plasma Phys. Controlled Fusion* **64**, 5, 054002 (2022).
5. Hasan, S.; Prelas, M. A. Molybdenum-99 production pathways and the sorbents for 99Mo/99mTc generator systems using (n, γ) 99Mo: a review. *SN Applied Sciences* **2020**, 2(11), 1782. Springer.
6. T. Hayakawa, Y. Hatsukawa, T. Tanimori, ^{95g}Tc and ^{96g}Tc as alternatives to medical radioisotope ^{99m}Tc , *Heliyon* **4**, 1 (2018).
7. M.U. Khandaker, M.S. Uddin, K.S. Kim, Y.S. Lee, G.N. Kim, Measurement of cross-sections for the (p,xn) reactions in natural molybdenum, *Nucl. Instrum. Methods Phys. Res. B* **262**, 171–181 (2007).
8. M.H. Jasim, M.M. Abbas, M.M. Jawad Al-Khalissi, Proton Induced Nuclear Excitation Functions of $^{100}\text{Mo}(p,2n)^{99m}\text{Tc}$ Reaction used as a Tracer in Nuclear Medicine, *Iraqi J. Sci.* **2024**, 4732–4739.
9. A.N. Shmelev, G.G. Kulikov, B.K. Kozhahmet, E.G. Kulikov, V.A. Apse, Use of molybdenum as a structural material of fuel elements for improving nuclear reactors safety, *Kerntechnik* **81**, 596–598 (2016).
10. A.N. Shmelev, B.K. Kozhahmet, Use of molybdenum as a structural material of fuel elements for improving the safety of nuclear reactors, *J. Phys.: Conf. Ser.* **781**, 012022 (2017).
11. Ziegler, J. F. Stopping and range of ions in matter SRIM-2003. www.srim.org, **2003**.
12. <http://www.tifr.res.in/~pell/lamp.html>.
13. N. Otuka, B. Lalremruata, M.U. Khandaker, A.R. Usman, L.R.M. Punte, Uncertainty propagation in activation cross section measurements, *Radiat. Phys. Chem.* **140**, 502–510 (2017).
14. F. Tárkányi, F. Ditroi, A. Hermanne, S. Takács, A.V. Ignatyuk, Investigation of activation cross-sections of proton induced nuclear reactions on natMo up to 40 MeV: new data and evaluation, *Nucl. Instrum. Methods Phys. Res. B* **280**, 45–73 (2012).
15. J. Červenák, O. Lebeda, Experimental cross-sections for proton-induced nuclear reactions on natMo, *Nucl. Instrum. Methods Phys. Res. B* **380**, 32–49 (2016).
16. O. Lebeda, M. Pruszyński, New measurement of excitation functions for (p,x) reactions on natMo with special regard to the formation of ^{95m}Tc , $^{96m+g}\text{Tc}$, ^{99m}Tc and ^{99}Mo , *Appl. Radiat. Isot.* **68**, 2355–2365 (2010).

17. A. Elbinawi, M. Al-Abyad, I. Bashter, U. Seddik, F. Ditroi, Study of proton induced nuclear reactions on molybdenum: cross section measurements and theoretical calculations, *Radiochim. Acta* **108**, 1, 1–9 (2019).
18. A.A. Ahmed, A. Wrońska, A. Magiera, R. Misiak, M. Bartyzel, J.W. Mietelski, B. Wąs, Study of ^{99}Mo and long-lived impurities produced through (p,x) reactions in natMo, *Radiat. Phys. Chem.* **190**, 109774 (2022).
19. A.A. Alharbi, J. Alzahrani, A. Azzam, Activation cross-section measurements of some proton induced reactions on Ni, Co and Mo for proton activation analysis (PAA) purposes, *Radiochim. Acta* **99**, 12, 763–770 (2011).
20. A.A. Anees Ahmed, A. Wrońska, A. Magiera, M. Bartyzel, J.W. Mietelski, R. Misiak, B. Wąs, Reexamination of proton-induced reactions on natMo at 19–26 MeV and study of target yield of resultant radionuclides, (2019).
21. M. Bonardi, C. Birattari, F. Groppi, E. Sabbioni, Thin-target excitation functions, cross-sections and optimised thick-target yields for natMo (p,xn) 94g , 95m , 95g , 96 (m+g) Tc nuclear reactions induced by protons from threshold up to 44 MeV. No Carrier Added radiochemical separation and quality control, *Appl. Radiat. Isot.* **57**, 5, 617–635 (2002).
22. W. Zhao, Y. Weixiang, H. Xiaogang, L. Hanlin, Excitation functions of reactions from d+ Ti, d+ Mo, p+ Ti and p+ Mo, (1998).
23. S. Takács, A. Hermanne, F. Ditrói, F. Tárkányi, M. Aikawa, Reexamination of cross sections of the $^{100}\text{Mo}(\text{p},2\text{n})^{99\text{m}}\text{Tc}$ reaction, *Nucl. Instrum. Methods Phys. Res., Sect. B* **347**, 26–38 (2015).
24. P. Chodash, C.T. Angell, J. Benitez, E.B. Norman, M. Pedretti, H. Shugart, E. Swanberg, R. Yee, Measurement of excitation functions for the natMo(d,x) ^{99}Mo and natMo(p,x) ^{99}Mo reactions, *Appl. Radiat. Isot.* **69**, 1447–1452 (2011).
25. E. Lamere, M. Couder, M. Beard, A. Simon, A. Simonetti, M. Skulski, G. Seymour, P. Huestis, K. Manukyan, Z. Meisel, et al., proton-induced reactions on molybdenum, *Phys. Rev. C* **100**, 034614 (2019).
26. V.N. Levkovski, cross sections of medium mass nuclide activation ($A = 40 - 100$) by medium energy protons and alpha-particles ($E = 10 - 50$ MeV), *Inter-Vesi, Moscow, USSR* (1991).
27. T. Matsuzaki, H. Sakurai, ^{99}Mo production via $^{99}\text{Tc}(\mu^-, \nu)$ ^{99}Mo reaction with recycled ^{99}Tc , *J. Radioanal. Nucl. Chem.* **333**, 11, 6007–6014 (2024).
28. M.C. Lagunas-Solar, P.M. Kiefer, O.F. Carvacho, C.A. Lagunas, Y.P. Cha, Cyclotron production of NCA $^{99\text{m}}\text{Tc}$ and ^{99}Mo . An alternative non-reactor supply source of instant $^{99\text{m}}\text{Tc}$ and $^{99}\text{Mo} \rightarrow ^{99\text{m}}\text{Tc}$ generators, *Int. J. Radiat. Appl. Instrum. A* **42**, 643–657 (1991).